PCCP

Accepted Manuscript

ROYAL SOCIETY OF CHEMISTRY

www.rsc.org/pccp

PCCP

RSCPublishing

PAPER

Improving the As(III) adsorption on graphene based surfaces: impact of the chemical doping

Cite this: DOI: 10.1039/xoxxoooooox

Diego Cortés-Arriagada[a,*] and Alejandro Toro-Labbé[a]

Received ooth January 2012,
Accepted ooth January 2012

DOI: 10.1039/xoxxoooooox

www.rsc.org/

On the basis of quantum chemistry calculations, the adsorption of As(III) onto graphene based adsorbents has been studied. The energetic and molecular properties that characterize the adsorption has been analyzed, and new adsorbents were proposed. The experimentally reported inefficient adsorption of As(III) by intrinsic graphene is theoretically characterized by a low adsorption energy (~0.3 eV), which is decreased by solvent effects. Two stable conformations were found for the adsorbent—adsorbate systems. The As(III) removal by unmodified oxidized graphene (GO) reaches a medium size adsorption strength (<~0.8 eV), still remaining low for high removal efficiency from a water environment. While the As(III) adsorption onto boron, nitrogen and phosphorous doped graphene is not favored with respect to the pristine adsorbent, aluminium, silicon and iron embedded graphene can adsorb As(III) by both chemical and physical interactions with high adsorption energies (> ~1 eV), even stable considering a solvent environment. The efficiency of the adsorbents for As(III) removal is sorted as Al-G>Fe-G>>Si-G>>GO>>G. Therefore, Al, Si and Fe doped graphene are considered as potential materials for efficient As(III) removal.

1. Introduction

Arsenic is one critical pollutant whose control is an environmental matter for government agencies in the world. The occurrence of this pollutant has its origin both natural and anthropogenic sources; natural sources are associated with geochemical characteristics and geology of grounds; pollution from the human activity comes from the mining wastes, landfills, arsenic-based pesticides, smelting of metal ores, wood preservatives, among others[1]. The water soluble species arsenite (As(III)) and arsenate (As(V)) are responsible for water pollution, and the chronic use of arsenic containing drinking waters cause cutaneous lesions, kidney and skin cancer, cardiovascular diseases, abortions, splenomegaly, disturbances in the nervous system, among others[2-10]. The trivalent specie is the most dangerous due to its toxicity and high mobility from solid surfaces, being 60 times more toxic compared to As(V)[11]. Then, development of processes allowing the control and removal of arsenic in the environment constitutes an important effort: some recent techniques for removal and/or degradation of arsenic involve extraction on macroporous materials and minerals[12-15], nanofiltration[16,17], electrocoagulation[18,19], and use of metallic nanoparticles as adsorbents[20].

Graphene has been one of the most important discovered materials, possessing useful properties as high mechanical strength, and high thermal and electronic conductivity[21-24]. Moreover, its straightforward synthesis from oxidized graphite and its lamellar structure confers graphene (and its nanocomposites) advantages for solid phase extraction of pollutant compared with other carbon allotropes as the carbon nanotubes (CNTs), with ever better desorption properties to account for the recovery of the adsorbent material[25]; for instance, graphene possess ability for the removal of neutral, ionic and cationic inorganic pollutants from aqueous solutions as Pb, Cd, As, Cr, Hg, and Co, among others[25]. At this regards, graphene based materials are reported as efficient for removal and detection of arsenic from aqueous sources, unlike pristine (or intrinsic) graphene which appears to be inefficient to interact with arsenic[25-37]. By mixing iron minerals with graphene and oxidized graphene, some nanocomposites has been obtained for arsenic removal which allow a high adsorption capacity from drinking waters and low adsorbent aggregation, with the advantage that can be removed from solution by simple and energy-saving magnetic methods[27,28,33]. Other graphene based material for improved arsenic removal include composites formed with layered double hydroxides and hydrated zirconium oxides[35,36]. On the other hand, graphene doping has also theoretically proven to be a useful method to improve the adsorption/sensing of harmful molecules such as NH_3, NO, NO_2, dioxin and formaldehyde[38-41]. Thus graphene doped material can be potential candidates to arsenic removal but experimental and theoretical studies are necessaries to account for its applicability.

In this article, taking into account the higher toxicity of arsenite compared with arsenate, quantum chemistry is used to understand the As(III) adsorption onto graphene based adsorbents, starting with the inefficient adsorption on pristine graphene, its interaction onto oxidized graphene, and the possibility of adsorption onto doped graphene. Dispersion force corrections were used for an accurate description of long-range interactions, and solvent effects were included to account for removal efficiency from a water environment.

2. Methodology

The $As(OH)_3$ (or arsenous acid, H_3AsO_3) form of arsenite was selected for this study because this was found to be dominant in neutral waters until pH=9.2[42,43]. As graphene model was used a finite graphene lattice ($C_{94}H_{24}$) with the dangling bonds at the edges saturated with hydrogen atoms. Well converged adsorption energies were obtained on this adsorbent model. B, N, Al, Si, P and Fe were used as dopants in embedded graphene, with a dopant concentration below 5%, which has been experimentally reached[44,45]. The oxidized graphene systems were built according to experimental analysis suggesting hydroxyl and epoxide groups attached to the basal plane, and carbonyl and carboxyl functionalized at edges[46-50].

Density functional theory (DFT) calculations were done using the PBE functional[51,52]; the Ahlrichs polarized double zeta basis set was used; a polarized triple-zeta basis set was adopted for As and Fe. The DFT-D3 method was used to include the effects of dispersion forces[53,54] in combination with the Becke-Johnson damping scheme to avoid repulsive interatomic forces at short distances[55,56]. The performance of the PBE-D3 method was checked with the dispersion correction by the non-local (NL) DFT method which uses the electron density to obtain the long-range dispersive energy contribution for the energy. In this case, PBE functional is combined with the non-local term of the VV10 functional containing refitted parameters[57,58]. NL correction was done for the PBE-D3 optimized structures as proposed in benchmark studies[58]. Adsorption energies of **1a-1b** systems determined by the PBE-D3 and PBE-NL methods have a difference of up to 0.01 eV, indicating the good agreement between the methods, even with differences of up to ~0.1 eV compared with those obtained at the MP2/cc-pVTZ level, which explicitly include dispersion effects. These results make us select PBE-D3 as a reliable method for this study taking into account computational efficiency and accuracy.

Adsorption energies (E_{ads}) were computed as:

$$E_{ads} = E_{adsorbent} + E_P - E_{adsorbent-P} \quad (1)$$

where, $E_{adsorbent}$, E_P and $E_{adsorbent-P}$ correspond to the total energies of the adsorbent, pollutant, and adsorbent-pollutant systems, respectively. A positive value of E_{ads} indicates stability for the adsorbent-adsorbate systems. Basis set superposition error was determined by means of the standard counterpoise correction[59]. Implicit solvent effects were included by the universal solvation model (SMD) method[60].

To ensure the adsorbate-adsorbent stability, molecular dynamics trajectories via Verlet velocity algorithm[62] were carried-out at 300 K on the DFT optimized systems, using the Berendsen thermostat[63]. Implicit solvent effects were included with the COSMO model[61]. The potential was determined "on-the-fly" at the semiempirical PM6 level[64] as used to analyze adsorption stability onto graphene of 4-chlorophenol and bisphenol-A[65,66]. The time-step for all simulations was 0.5 fs, and 5.0 fs were used as production; data were collected for statistics after 1 fs of both heating and equilibrium.

All the calculations were performed in the electronic structure program ORCA 3.0[67]. Semiempirical calculations were carried-out in the MOPAC2012 program[68]. Results were analyzed in the graphical user interface Gabedit 2.4.8[69], Chemcraft 1.7[70] and the wavefunction analyzer Multiwfn[71]. Atomic charges and bonding characteristics were obtained from the NBO 6.0 program[72].

Table 1 Adsorption energies (E_{ads}) in gas phase (in parenthesis with water as solvent), percentage of contribution of van der Waals interactions ($\%E_{vdW}$), and pollutant charge after adsorption (Q_P). Energies in eV. G and GO stand for graphene and oxidized graphene, respectively; for GO, the superscript depicts the analyzed functional group.

System	E_{ads}	$\%E_{vdW}$	Q_P
with pristine graphene			
1a: G···$As(OH)_{3a}$	0.31 (-0.09)	100%	0.008
1b: G···$As(OH)_{3b}$	0.32 (-0.06)	100%	0.009
with doped graphene			
2a: Al-G···$As(OH)_{3a}$	1.66 (1.33)	21%	0.158
2b: Al-G···$As(OH)_{3b}$	1.64 (1.32)	23%	0.182
3a: Si-G···$As(OH)_{3a}$	1.01 (0.85)	38%	0.165
3b: Si-G···$As(OH)_{3b}$	0.97 (0.78)	42%	0.206
4a: P-G···$As(OH)_{3a}$	0.28 (0.09)	100%	0.008
4b: P-G···$As(OH)_{3b}$	0.35 (0.17)	100%	0.009
5a: Fe-G···$As(OH)_{3a}$	1.61 (1.28)	23%	0.189
5b: Fe-G···$As(OH)_{3b}$	1.58 (1.25)	27%	0.191
with oxidized graphene			
6a: $GO^{epoxide}$···$As(OH)_3$	0.44 (0.24)	69%	-0.026
6b: $GO^{hydroxyl}$···$As(OH)_3$	0.66 (0.36)	63%	0.010
6c: $GO^{carboxyl}$···$As(OH)_3$	0.78 (0.50)	17%	0.034
6d: $GO^{carbonyl}$···$As(OH)_3$	0.54 (0.12)	32%	-0.038

3. Results and Discussion

3.1 Adsorption on intrinsic graphene

In the first place, it is analyzed the $As(OH)_3$ physisorption on pristine graphene. Table 1 shows the adsorption energy, the contribution of dispersion forces, and the pollutant charge after the adsorption.

Two stable conformations were found (Figure 1). In the **1a** conformation, the molecule is "seated" onto the adsorbent surface with one of the As-O bonds directed away from the graphene surface. Arsenic is placed at an intermolecular distance of 3.34 Å from the adsorbent. Note that As-OH distances and HO-As-OH angles in the isolated $As(OH)_3$ molecule are calculated to be $d_{As\text{-}OH}$=1.82 Å and $\angle_{O\text{-}As\text{-}O}$=97°, respectively, showing a C_3 symmetry, in agreement with DFT studies[73]. The "seated" conformation changes the $\angle_{O\text{-}As\text{-}O}$ in $As(OH)_3$, distorting its pyramidal geometry, while bond lengths are almost unchanged. In the case of the **1b** conformation, $As(OH)_3$ is adsorbed "lying-down" with all the hydroxyl groups directed toward the adsorbent surface, while the arsenic atom is placed on the top of a carbon atom at 3.98 Å. Angles and bond lengths of the adsorbate appear nearly unchanged in this conformation. Both **1a** and **1b** the adsorption energy appears similar and slightly stable, with values of 0.31 and 0.32 eV, due 100% to long-range interactions, which would be not enough to stabilize the adsorption in an aqueous environment due to the expected lowering by the solvation energy. The latter is in

agreement with the low efficiency of the intrinsic graphene for arsenic removal[25], thus expecting a low energy barrier for the diffusion through the adsorbent surface. Moreover, both **1a** and **1b** the pollutant charge (Q_P) after adsorption of the order of $+1{\cdot}10^{-2}|e|$ (Table 1), indicating some of electronic polarization toward the adsorbent but absent of a net charge transfer process. Note that in later analysis, we will refer to "seated" and "lying-down" conformations as "**a**" and "**b**".

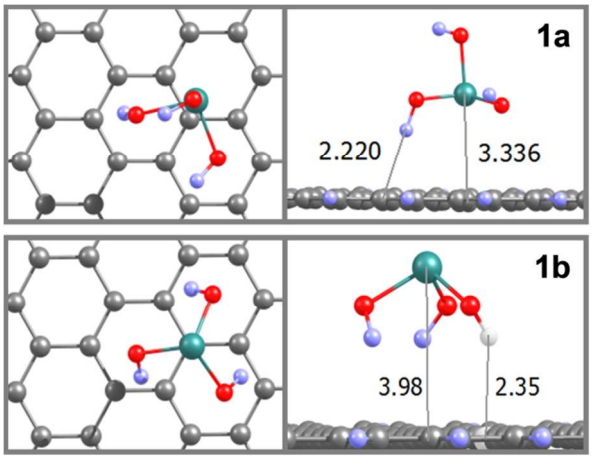

Fig. 1 Side and top view of the optimized molecular structures of $As(OH)_3$ adsorbed onto graphene; two interaction modes were obtained (**1a**, **1b**). Distances in angstroms (Å).

The non-covalent interaction index (NCI)[74,75] was used to observe the weak interactions dominating the physisorption. NCI is based on the reduced density gradient s and the electron density ρ:

$$s = \frac{\nabla\rho}{2(3\pi^2)^{1/3}\rho^{4/3}} \quad (5)$$

This quantity is related to long-range interactions to low electron density regions. By using the Bader´s atoms in molecules theory[76], points in the low density region are related to the sign of the second largest eigenvalue of the Hessian matrix of electron density (λ_2), where λ_2 gives information about the chemical interactions[74,75]. According with the NCI scheme, weak interactions are found for $\lambda_2 \sim 0$. The NCI surface (Figure 2) show that both **1a** and **1b** systems, the dispersion forces taking place above the π-density of three benzene type rings in according with the relative same values of the adsorption energies even when conformation are different. This pattern will be compared with further analysis.

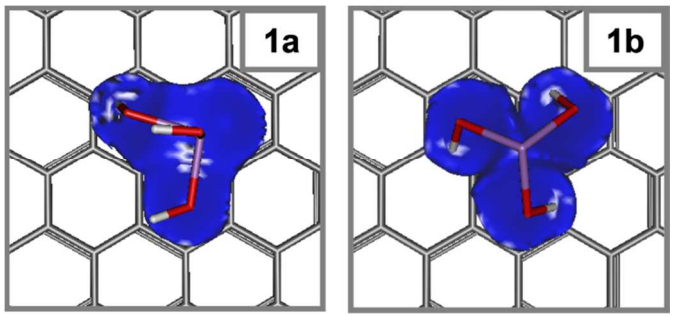

Fig. 2 NCI surface of weak interactions in the **1a-1b** systems. NCI plotting: s=0.7, λ_2=[-0.015; 0.010].

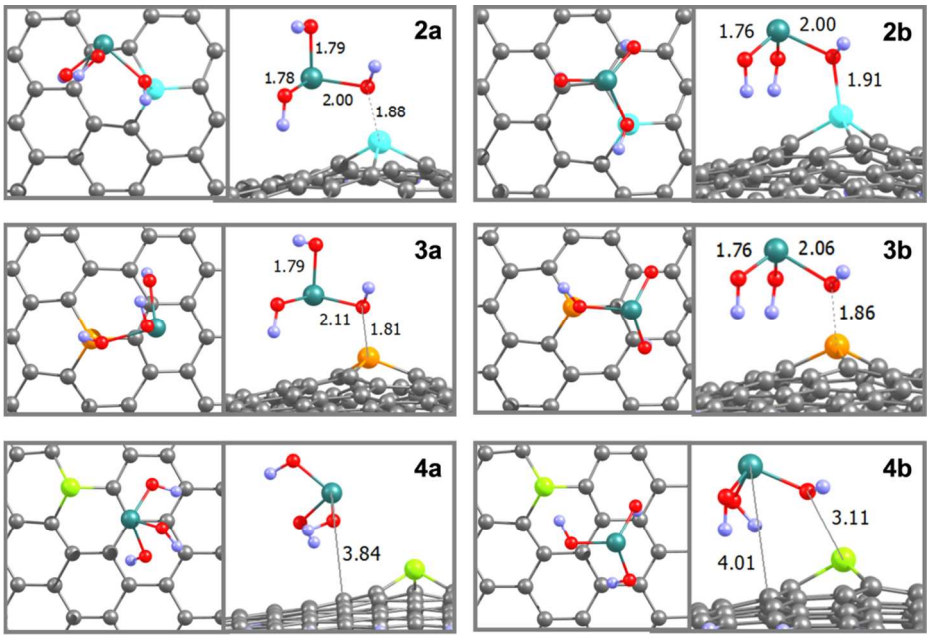

Fig. 3 Side and top view of the optimized molecular structures of $As(OH)_3$ adsorbed onto doped graphene with aluminum (**2**), silicon (**3**), and phosphorous (**4**); two interaction modes were obtained (**a**, **b**). Distances in angstroms (Å).

3.2 Adsorption on doped graphene

To account for an efficient arsenite adsorption on the doped graphene, it is necessary to use dopants allowing chemical interactions with the pollutant. The graphene doping with nitrogen and boron retain the planarity and sp^2 hybridization of graphene and they do not offer chemical interaction with $As(OH)_3$; they shows long-range interactions of the order of 0.33-0.44 eV (see supplementary information). On the other hand, high structural effects on the adsorbent surface are reached with third-row dopants (Al, Si, and P) due to theirs larger atomic radius compared to carbon. In these cases, dopants expand-out of the plane increasing reactivity and binding with adsorbates[77-79], mainly by reducing the structural work associated with the activation energies[80,81]. According with the increased atomic radius compared to carbon, the isolated Al, Si and P-doped adsorbents were obtained with C-Al, C-Si and C-P bond distances of $d_{C\text{-}Al}$=1.86, $d_{C\text{-}Si}$=1.76 and $d_{C\text{-}P}$=1.78 Å, respectively, compared to $d_{C\text{-}C}$=1.42 Å of graphene, which are in good agreement with previous DFT calculations[77-79,82].

The $As(OH)_3$ interaction onto Al and Si-doped graphene (Fig. 3) is characterized with high adsorption energies due to a dopant-oxygen bond. For Al-doped graphene, the **2a** and **2b** conformations show the Al-O bond with distances of $d_{Al\text{-}O}$=1.88 and 1.91 Å, respectively; $d_{Al\text{-}O}$ distance is slightly lower for **2a** in agreement with difference in stability by 0.02 eV with respect to **2b**. In both conformations, the Al-O interaction causes an increase of the bond length of the interacting As-O bond from 1.82 to ~2.00 Å. On the other hand, in the Si-doped case, **3a** and **3b** systems have Si-O bond lengths of $d_{Si\text{-}O}$=1.81 and 1.86 Å, respectively, with adsorption energies of 1.01 and 0.97 eV, respectively; the "seated" conformation is slightly more stable in agreement with a lower $d_{Si\text{-}O}$ compared to "lying-down". The interacting As-O bond is elongated from $d_{As\text{-}O}$=1.82 Å to ~2.10 Å. Finally, onto P-doped graphene, any dopant-pollutant interaction was observed, and physisorption take place onto the graphitic sites with low adsorption energies, geometrical parameters and charge transfer as in the intrinsic adsorbent. These results suggest that Al and Si doped graphene can serve as efficient materials to the efficient adsorption of the mobile As(III).

In other respects, the dispersion force contribution to adsorption energies in the Al-G···$As(OH)_3$ systems is about 21-23%, noting the important chemical nature of the interaction in these cases, also characterized by electron transfer of up to ~0.2*e* toward the adsorbent. Besides, in the Si-G···$As(OH)_3$ systems, dispersion forces contribute up to ~42% for the adsorption strength, and electron transfer toward the adsorbent occurs (up to ~0.2*e*). Note that the different pattern of the NCI surfaces of the Al- and Si-G···$As(OH)_3$ systems compared to G···$As(OH)_3$ (Fig. 4) are in agreement with a low/medium contribution of weak interactions allowing the adsorption.

In order to account for the nature of chemical interactions, the NBO analysis was performed. In the Al and Si-doped graphene, Al ($[Ne]3s^23p^1$) and Si ($[Ne]3s^23p^2$) develop sp^2 hybridization to bond to graphene. As a result, $As(OH)_3$ behaves as a Lewis base, hence a lone pair electron of the oxygen containing group interacts with the non-hybridized and low occupied *3p* lone pair orbital of the dopant to form an adduct with coordinate covalent bond (Fig. 5). The occupation of these dopant lone vacant orbitals are of 0.23*e* and 0.74*e* for Al and Si, respectively, hence allowing donor-acceptor interactions, and the bonding stability is decreased as increase occupation number of the lone vacant orbital; the latter explains the lower adsorption energy using Si-G compared to those using Al-G. In the case of P-doped graphene, although this is proposed to have increased reactivity for nucleophilic attack[77], any P-pollutant interaction was found. According with the electronic configuration of P ($[Ne]3s^23p^3$), sp^3 hybridization between *3s* and *3p* orbitals of phosphorous forms three half-filled orbitals available to form σ-bonding with carbon atoms in the adsorbent, while a high occupied non-bonding lone pair (1.73*e*) is formed (unlike Al-G and Si-G). The latter causes that P stops behaving as a Lewis acid and not set bonding with donor lone pair in $As(OH)_3$, favoring an interaction 100% by dispersion forces as observed from the NCI surface (Fig. 4).

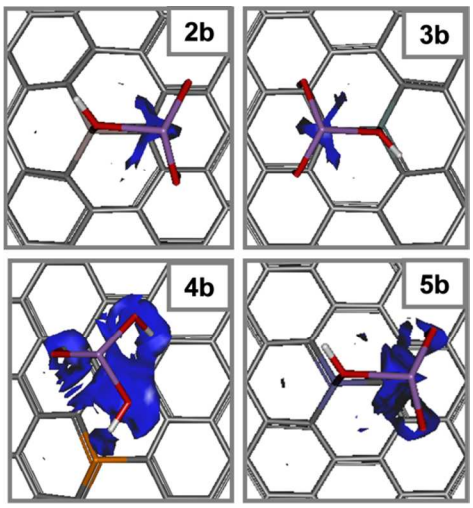

Fig. 4 NCI surface of weak interactions for the adsorption of doped-G···$As(OH)_3$ systems. The "lying-down" conformations were selected. NCI plotting: s=0.7, λ_2=[-0.010;+0.010].

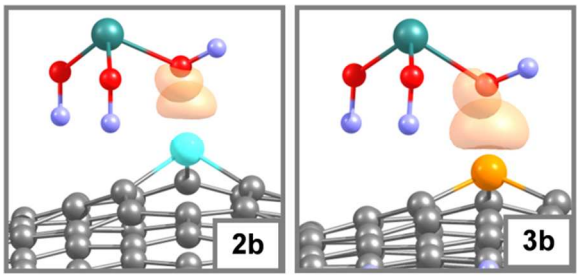

Fig. 5. Bonding due to donor-acceptor interactions between oxygen and dopant atom in **2b**-**3b** systems.

We try for doping with a fourth row metal as Fe. The Fe embedded graphene has shown high adsorption energies toward oxygen containing molecules as CO (1.38 eV) and O_2 (1.65 eV)[83], thus promising to adsorption of As(III) by chemical interaction at neutral conditions, even with a low-cost and benign behavior with the environment[83]. For this adsorbent, diffusion barrier was calculated at 6.78 eV, indicating the stability of the support[83]. For the isolated adsorbent, C-Fe bond distance was found to be $d_{C\text{-}Fe}$=1.77 Å, with Fe expanding out of the adsorbent plane, in good agreement with DFT calculations[84].

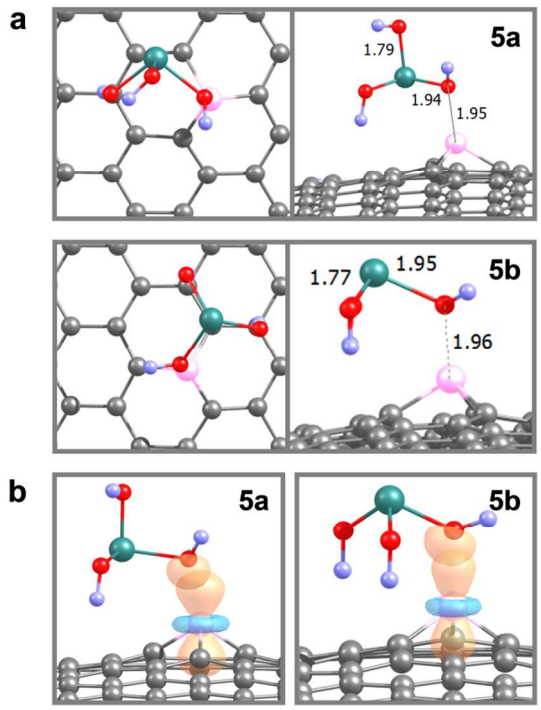

Fig. 6. a) Structure of Fe-G···$As(OH)_3$ systems (**5a**, **5b**). b) Bonding due to donor-acceptor interactions. Distances in angstroms (Å).

Figure 6a depicts the "seated" (**5a**) and "lying-down" (**5b**) conformations of the onto Fe-G···$As(OH)_3$ systems. Both conformations show closer adsorption energies of 1.61 (**5a**) and 1.58 eV (**5b**), indicating formation of chemical bonding. In average, the Fe-O bond length is of ~1.95 Å, and the O-As bond is elongated from 1.82 to ~1.95 Å. Both energy as geometrical parameters are comparable with the $As(OH)_3$ chemisorption onto FeS_2 pyrite, where bidentate conformations with Fe-O bonding were computed with adsorption energy of 1.44 eV[73]. The Fe-G···$As(OH)_3$ interaction proceeds with a charge transfer from the pollutant molecule to the adsorbent of 0.19*e*, delocalizing the charge density on the carbon atoms surrounding the dopant, retaining the dopant net charge to Q_{Fe}=+0.4|*e*| as in the isolated Fe-G adsorbent. In addition, dispersion forces have a lower contribution of the order of 23-27%, taking place outside the site occupied by the dopant (Fig. S4). Nature of the chemical interaction show that Fe behaves as a Lewis acid and the strong bonding is established by coordination between an oxygen lone pair electron and the low-occupied Fe $3d_z^2$ orbital in the dopant (Fig. 6b). Therefore, Fe-doped graphene is proposed as a good candidate for As(III) removal due to its high adsorption energy towards the $As(OH)_3$ molecule.

3.3 Adsorption on oxidized graphene

Graphene oxide (GO) has shown a low efficiency for arsenic removal[25], and in this section we try to understand this experimental fact. The conformations for the GO···$As(OH)_3$ are depicted in Fig. 7. The $As(OH)_3$ adsorption on the basal plane of graphene oxide would be reached onto epoxide (**6a**) and hydroxyl groups (**6b**)[46-50]. In addition to the dispersion forces, adsorption is improved by hydrogen bond interactions up to 37%. Onto an epoxide group, $As(OH)_3$ shows stabilization by hydrogen bonds of the order of 1.93-1.95 Å, increasing the adsorption energy to 0.44 eV. An enhanced adsorption appears on a hydroxyl group, reaching a strength of 0.66 eV, mainly because hydrogen bond interaction are strengthening, in agreement with shorter distances (1.75-1.78 Å) compared to the found ones onto the epoxide functionalized graphene. Interaction with functional groups at the edges of GO models (**6c**, **6d**) is enhanced by hydrogen bonds, with some of contribution from dispersion forces up to 32%. Interaction with carboxyl group appear to be the most stable among the all oxygen containing functional groups, with E_{ads}=0.78 eV; hydrogen bond lengths of 1.53-1.87 Å are observed, which are established both the C=O and OH moiety at the carboxyl group. Adsorption near to a carbonyl group appears with an adsorption energy of 0.54 eV and intermolecular C=O···H distances of 1.97-2.07 Å, indicative of a decreased bonding strength.

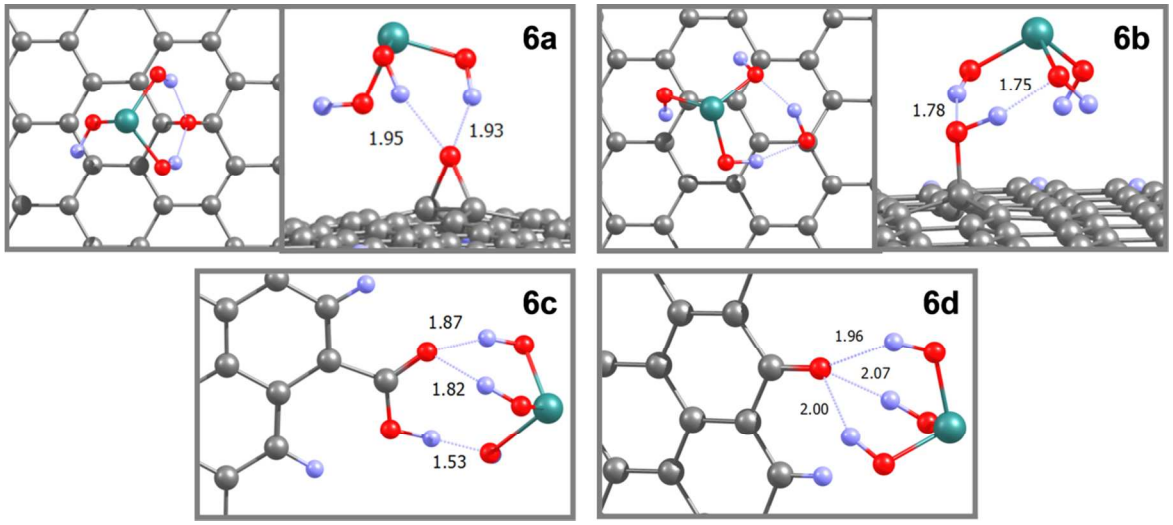

Fig. 7 Side and top view of the optimized molecular structures of $As(OH)_3$ adsorbed onto oxidized graphene containing epoxide (**6a**), hydroxyl (**6b**), carboxyl (**6c**) and carbonyl (**6d**) groups. Distances in angstroms (Å).

These results show that the As(III) adsorption onto oxidized graphene is reached with a medium strength, so that stability is affected by solvation energies as noted from Table 1. Even by considering the adsorption onto extended and regular functionalized GO models, a low increase in the adsorption energies of up to 0.28 and 0.10 eV was obtained for adsorption on the bulk and edges, respectively (see supplemental material). Therefore, the chemical interaction between pollutant and the adsorbent is the better strategy to an effective As(III) removal. In this sense, chemical modification of graphene oxide with ferric-oxides and iron-based nanoparticles have been a useful experimental technique to increase removal of arsenite and arsenate from contaminated waters[25,27,28,30,33,34], where it is expected chemical interactions between oxygen containing groups of arsenous acid with iron, similar as takes place onto Fe-doped graphene. These graphene oxide composites perform with a adsorption capacity toward As(III) of 13.1 to 23.8 mg/g. Even better, graphene oxide modification with hydrated zirconium oxide ($ZrO(OH)_2$) allows to enhance removal of As(III) up to 95.2 mg/g in a wide pH range with low equilibrium times[36].

3.4 Adsorption stability

In order to insure the stability of the dopant-pollutant interaction in the efficient adsorbents (**2**, **3** and **5)**, molecular dynamics trajectories were performed at 300 K. The analysis was focused both the dopant-O and As-O bond distances by means of the radial pair distribution function ($g_{ab}(r)$) (Fig. 8), which allows determining the distribution of distances between two atoms in the overall trajectory. Results shows that in dynamic conditions, both "seated" and "lying-down" conformations are modified due to kinetic energy, but the chemisorption remains as a strong interaction. The $g_{ab}(r)$ function for dopant-oxygen bond is retained in the range $d_{Al\text{-}O}$=[1.9-2.2Å], $d_{Si\text{-}O}$=[1.7-1.9Å] and $d_{Fe\text{-}O}$=[1.7-1.9Å], indicating that the chemical bond is even strong at ambient conditions. Moreover, the As-O bond must be in a bond range to insure a low labile character of the interacting hydroxyl group. Indeed, the As-O bond length is retained in a range of $d_{As\text{-}O}$=[1.7-2.1 Å] between all the analyzed systems.

3.5 Solvent effects

As earlier discussed, the solvation energy can reduce drastically the arsenic removal, especially on those adsorbents showing low/medium adsorption strength. With respects to the solvent effects, has been determined that the H_2O molecules are physisorbed onto graphene with energies <100 meV per molecule, at distances of 3.50-3.25 Å from the surface, forming clusters[85-87]. Although a decrease of the adsorption energies is expected in a water environment, the latter suggest that the pollutant will be structurally stabilized by forming of water clusters surrounding the adsorbate after its diffusion toward the adsorbent site. To account for these solvent effects, we first obtain the adsorption energies including an implicit solvent environment (Table 1). From Table 1 is noted that the arsenite adsorption on the intrinsic and oxidized graphene turns unstable or low stable since solvation energy has an effect of ~0.3 eV on the all adsorption energies; thus low diffusion barriers for the desorption processes are expected, explaining because graphene and oxidized graphene are inefficient as arsenite adsorbents. On the other hand, the chemical interaction of $As(OH)_3$ on the doped adsorbents is enough to keep a strong adsorption even in a water environment, especially for the Al and Fe doped graphene, with adsorption energies in the range of 1.33-0.78 eV. At first glance, we can sort the efficiency of the adsorbents for As(III) removal from a water environment as *Al-G>Fe-G>>Si-G>>GO>>G*.

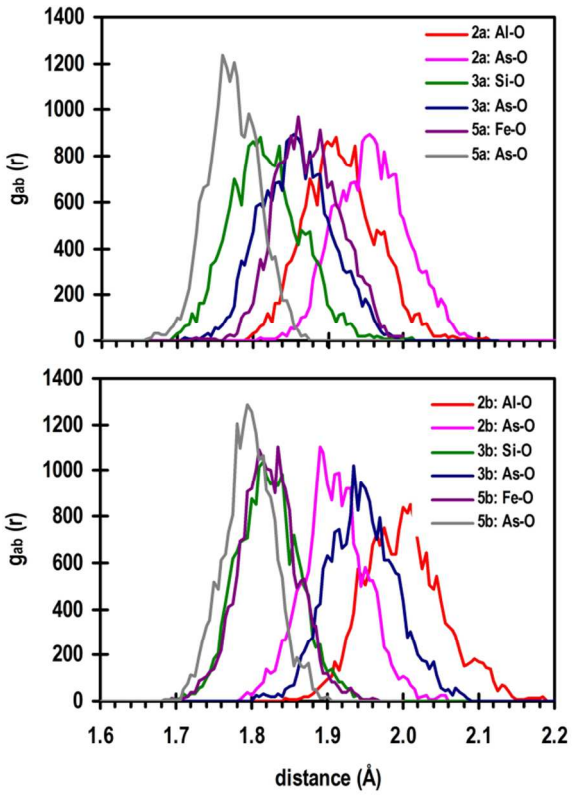

Fig. 8. Radial pair distribution function ($g_{ab}(r)$) of bond distances in **2**, **3** and **5**. 20000 conformations per system were used for statistics, during a time t=5.0 ps at 300K.

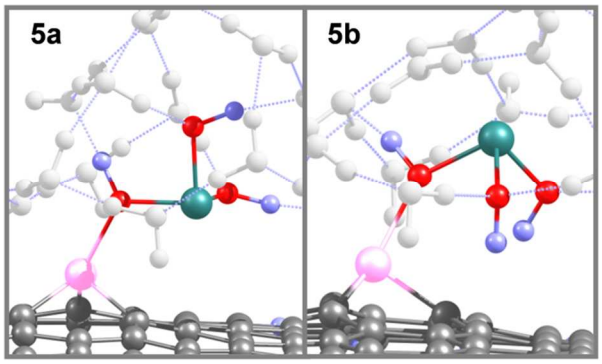

Fig. 9. "Seated" and "lying-down" conformations of the Fe-G···$As(OH)_3$ systems in a solvent environment; 15 H_2O molecules are depicted in white with pointed hydrogen bonds. Si and Al-G···$As(OH)_3$ systems are included as supplementary material.

To get more insights about the structural effects of solvent molecules in the adsorbent-adsorbate systems, an explicit/implicit methodology was taken in a second stage by surrounding the adsorbate with 15 H_2O molecules and optimizing the whole system in presence of the implicit solvent. It was observed that the H_2O molecules form a cluster surrounding the adsorbate (Fig. 9), but they slightly affect the conformations of the adsorbate as obtained in an isolated model, and they structurally stabilize the adsorption as suggested above. In addition, the interacting OH group of the pollutant slightly elongates its bond length, suggesting that the hydrogen atom of this group turns labile in presence of the solvent; it is expected that the arsenite in its $As(OH)_2O^-$ form, still remain adsorbed and stabilized onto the doped adsorbents due to the strong chemical bonding.

3.6 Charge density distribution

In this point, we discuss some aspects about the arsenite adsorption mechanism on the proposed adsorbents with high adsorption strength. The first step in the pollutant adsorption onto Al, Si and Fe-doped graphene must be involve some of long-range attractive forces to allow the pollutant diffusion to the adsorbent, mainly by a charge-controlled interaction. At this regard, molecular electrostatic potential (Fig. 10a) reveals the charge density distributions in the isolated systems by means of the negative (red color) and positive (blue color) charge excesses.

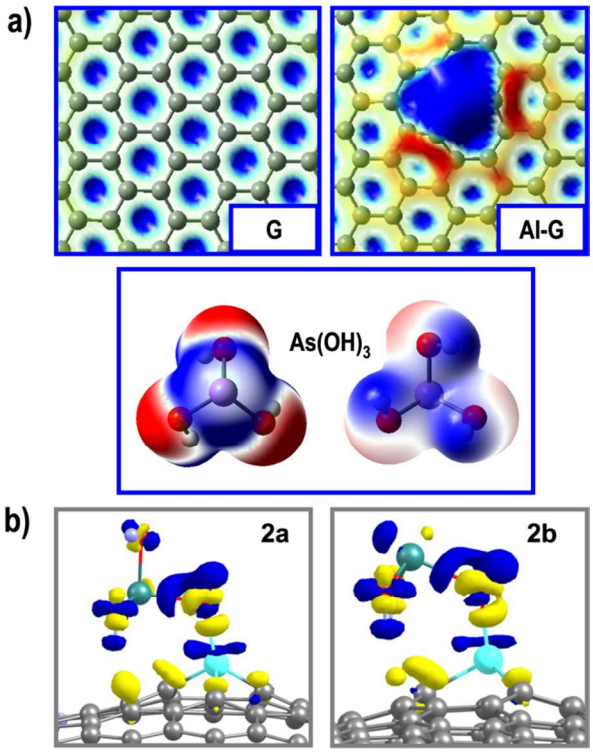

Fig. 10. a) Molecular electrostatic potential of $As(OH)_3$, graphene and Al-doped graphene. **b)** Fragmental electron density difference of **2a** and **2b** systems; colors stand for electron density decreasing (blue color) and electron density increasing (yellow color). As supplementary material are included **3** and **4** systems.

Figure 10a shows that in the $As(OH)_3$ molecule the negative charge is localized on the oxygen atoms (Q_O=–0.96|*e*|), while positive charge is mainly located in the arsenic (Q_{As}=+1.48|*e*|). The dopant atoms in the embedded graphene cause a positively charged site capable to interact with the negatively charged oxygen atoms in the pollutant; dopant charges appear to be Q_{Al}=+1.66|*e*|, Q_{Si}=+1.49|*e*| and Q_{Fe}=+0.40|*e*|, suggesting a better Coulombic interaction with the Al and Si-doped graphene. Therefore, the electrostatic interaction is expected to be the main mechanism whereby the $As(OH)_3$ reaches the site for chemisorption overcoming either the diffusion thought the solvent or from the graphene surface. In addition, the electrostatic interaction is clearly favored in the "seated" and "lying-down" configurations because of interaction with the arsenic atom is repulsive in nature.

The next step is the adduct forming when the $(OH)_b$ group (which is part of the dopant-O bond) is closed to the adsorption site. From the plotting of the fragmental electron density difference (Fig. 10b), the electron density distributions taking place before and after of the chemical interaction are observed. Taking the Al-G···$As(OH)_3$ system (**2**) as representative, it is observed that the chemisorption proceeds with a decrease of the electron density onto the aluminum atom and the As-$(OH)_b$ bond. Note that the electron density decreasing in the hydrogen of the $(OH)_b$ moiety indicates that this one must turn more labile that in the isolated $As(OH)_3$ molecule, which was noticeably noted above by simulations with explicit H_2O molecules. Moreover, the interacting oxygen atom (that behaves as a Lewis base) appears increasing its electron density; while, the carbon atoms surrounding the dopant increase its electron density and appear to interact with the electron deficient hydrogen atoms of the pollutant, favoring stabilization of the "seated" and "lying-down" conformations.

4 Conclusions

In summary, a quantum chemistry study was performed about the adsorption of trivalent arsenic onto graphene based adsorbents, contributing to understanding the interaction modes of the adsorbent-adsorbate systems, their stabilities at neutral conditions in water environments, and the role of the chemical doping to improve the adsorption strength. It was found that the inefficient adsorption of As(III) by intrinsic graphene is characterized by low adsorption energies (~0.3 eV), which turns even lower by solvation effects, which reduce the all adsorption energies by ~0.3 eV. Two stable interaction modes for the adsorbent-adsorbate systems were found on the all studied systems, showing a "seated" and "lying-down" conformation. The As(III) removal by unmodified oxidized graphene (GO) reaches a medium size adsorption strength (<~0.8 eV), still remaining low for high removal efficiency from water environments. The As(III) adsorption onto boron, nitrogen and phosphorous doped graphene shows a low improvement in adsorption energies with respect the pristine adsorbent (up to +0.1 eV). The aluminium, silicon and iron embedded graphene can adsorb As(III) by both chemical and physical interactions with high adsorption energies (> ~1 eV), even stable considering a solvent environment at ambient conditions. The efficiency of the adsorbents for As(III) removal from water is sorted as next *Al-G>Fe-G>>Si-G>>GO>>G*. We conclude that either Al, Si and Fe doped graphene are potential materials for efficient As(III) removal from polluted waters, even with a comparable efficiency as mineral based materials.

Acknowledgements

This work was supported by the project: FONDECYT Postdoctorado N°3140314, FONDECYT 1130072 and ICM grant N°120082.

Notes and references

[a] *Nucleus Millennium Chemical Processes and Catalysis; Laboratorio de Química Teórica Computacional (QTC), Departamento de Química-Física, Facultad de Química, Pontificia Universidad Católica de Chile, Av. Vicuña Mackenna 4860, Macul, Santiago, Chile.*

[*] *Email: dcortesr@uc.cl*

† Electronic Supplementary Information (ESI) available. See DOI: 10.1039/b000000x/

1 C. Jain and I. Ali, *Water Research*, 2000, **34**, 4304-4312.

2 R. Zaldivar, *Zentralblatt fur Bakteriologie. 1. Abt. Originale B, Hygiene, Krankenhaushygiene, Betriebshygiene, praventive Medizin*, 1980, **170**, 44-56.

3 M.-M. Wu, T.-L. Kuo, Y.-H. Hwang and C.-J. Chen, *American Journal of Epidemiology*, 1989, **130**, 1123-1132.

4 C.-H. Wang, C. K. Hsiao, C.-L. Chen, L.-I. Hsu, H.-Y. Chiou, S.-Y. Chen, Y.-M. Hsueh, M.-M. Wu and C.-J. Chen, *Toxicology and applied pharmacology*, 2007, **222**, 315-326.

5 Y. Chen, F. Parvez, M. Gamble, T. Islam, A. Ahmed, M. Argos, J. H. Graziano and H. Ahsan, *Toxicology and applied pharmacology*, 2009, **239**, 184-192.

6 J. Saha, A. Dikshit, M. Bandyopadhyay and K. Saha, *Critical reviews in environmental science and technology*, 1999, **29**, 281-313.

7 G. A. Soto-Peña, A. L. Luna, L. Acosta-Saavedra, P. Conde, L. López-Carrillo, M. E. Cebrián, M. Bastida, E. S. Calderón-Aranda and L. Vega, *The FASEB journal*, 2006, **20**, 779-781.

8 J. R. Meliker, R. L. Wahl, L. L. Cameron and J. O. Nriagu, *Environ Health*, 2007, **6**, 1-11.

9 P. P. Simeonova and M. I. Luster, *Toxicology and applied pharmacology*, 2004, **198**, 444-449.

10 D. Melak, C. Ferreccio, D. Kalman, R. Parra, J. Acevedo, L. Pérez, S. Cortés, A. H. Smith, Y. Yuan and J. Liaw, *Toxicology and applied pharmacology*, 2014, **274**, 225-231.

11 J. F. Ferguson and J. Gavis, *Water Research*, 1972, **6**, 1259-1274.

12 A. Gupta, V. S. Chauhan and N. Sankararamakrishnan, *Water Research*, 2009, **43**, 3862-3870.

13 J. Yang, H. Zhang, M. Yu, I. Emmanuelawati, J. Zou, Z. Yuan and C. Yu, *Advanced Functional Materials*, 2014, **24**, 1354-1363.

14 M. P. Asta, J. Cama, M. Martínez and J. Giménez, *Journal of hazardous materials*, 2009, **171**, 965-972.

15 J.-S. Kwon, S.-T. Yun, J.-H. Lee, S.-O. Kim and H. Y. Jo, *Journal of hazardous materials*, 2010, **174**, 307-313.

16 A. Figoli, A. Cassano, A. Criscuoli, M. Mozumder, M. T. Uddin, M. A. Islam and E. Drioli, *Water Research*, 2010, **44**, 97-104.

17 V. Nguyen, S. Vigneswaran, H. Ngo, H. Shon and J. Kandasamy, *Desalination*, 2009, **236**, 363-369.

18 N. Balasubramanian, T. Kojima, C. A. Basha and C. Srinivasakannan, *Journal of hazardous materials*, 2009, **167**, 966-969.

19 H. K. Hansen and L. M. Ottosen, *Separation Science and Technology*, 2010, **45**, 1326-1330.

20 S. R. Chowdhury and E. K. Yanful, *Journal of Environmental Management*, 2010, **91**, 2238-2247.

21 K. S. Novoselov, A. K. Geim, S. V. Morozov, D. Jiang, Y. Zhang, S. V. Dubonos, I. V. Grigorieva and A. A. Firsov, *Science*, 2004, **306**, 666-669.

22 C. Lee, X. Wei, J. W. Kysar and J. Hone, *Science*, 2008, **321**, 385-388.

23 S. Chen, Q. Wu, C. Mishra, J. Kang, H. Zhang, K. Cho, W. Cai, A. A. Balandin and R. S. Ruoff, *Nat Mater*, 2012, **11**, 203-207.

24 K. I. Bolotin, K. J. Sikes, Z. Jiang, M. Klima, G. Fudenberg, J. Hone, P. Kim and H. L. Stormer, *Solid State Communications*, 2008, **146**, 351-355.

25 Y. Cao and X. Li, *Adsorption*, 2014, **20**, 713-727.

26. X.-L. Wu, L. Wang, C.-L. Chen, A.-W. Xu and X.-K. Wang, *Journal of Materials Chemistry*, 2011, **21**, 17353-17359.

27 V. Chandra, J. Park, Y. Chun, J. W. Lee, I.-C. Hwang and K. S. Kim, *ACS nano*, 2010, **4**, 3979-3986.

28 K. Zhang, V. Dwivedi, C. Chi and J. Wu, *Journal of hazardous materials*, 2010, **182**, 162-168.

29 A. K. Mishra and S. Ramaprabhu, *Desalination*, 2011, **282**, 39-45.

30 J. Zhu, R. Sadu, S. Wei, D. H. Chen, N. Haldolaarachchige, Z. Luo, J. Gomes, D. P. Young and Z. Guo, *ECS Journal of Solid State Science and Technology*, 2012, **1**, M1-M5.

31 D. Nandi, K. Gupta, A. K. Ghosh, A. De, S. Banerjee and U. C. Ghosh, in *Nanotechnology for Sustainable Development*, Springer, 2014, pp. 149-162.

32 G. Ramesha and S. Sampath, *Sensors and Actuators B: Chemical*, 2011, **160**, 306-311.

33. G. Sheng, Y. Li, X. Yang, X. Ren, S. Yang, J. Hu and X. Wang, *RSC Advances*, 2012, **2**, 12400-12407.

34. S. Vadahanambi, S.-H. Lee, W.-J. Kim and I.-K. Oh, *Environ. Sci. Technol.*, 2013, **47**, 10510-10517.

35. T. Wen, X. Wu, X. Tan, X. Wang and A. Xu, *ACS applied materials & interfaces*, 2013, **5**, 3304-3311.

36 X. Luo, C. Wang, L. Wang, F. Deng, S. Luo, X. Tu and C. Au, *Chem. Eng. J.*, 2013, **220**, 98-106.

37 Y. Liu, Z. Huang, Q. Xie, L. Sun, T. Gu, Z. Li, L. Bu, S. Yao, X. Tu and X. Luo, *Sensors and Actuators B: Chemical*, 2013, **188**, 894-901.

38 Y. Chen, B. Gao, J.-X. Zhao, Q.-H. Cai and H.-G. Fu, *J Mol Model*, 2012, **18**, 2043-2054.

39 H. S. Kang, *Journal of the American Chemical Society*, 2005, **127**, 9839-9843.

40 X. Qin, Q. Meng and W. Zhao, *Surface Science*, 2011, **605**, 930-933.

41 H.-p. Zhang, X.-g. Luo, X.-y. Lin, X. Lu, Y. Leng and H.-t. Song, *Applied Surface Science*, 2013, **283**, 559-565.

42 M. L. Pierce and C. B. Moore, *Water Research*, 1982, **16**, 1247-1253.

43 G. A. Cutter, *Marine Chemistry*, 1992, **40**, 65-80.

44 L. Panchakarla, K. Subrahmanyam, S. Saha, A. Govindaraj, H. Krishnamurthy, U. Waghmare and C. Rao, *Advanced Materials*, 2009, **21**, 4726-4730.

45 R. Lv, Q. Li, A. R. Botello-Méndez, T. Hayashi, B. Wang, A. Berkdemir, Q. Hao, A. L. Elías, R. Cruz-Silva and H. R. Gutiérrez, *Scientific reports*, 2012, **2**.

46 A. Lerf, H. He, M. Forster and J. Klinowski, *The Journal of Physical Chemistry B*, 1998, **102**, 4477-4482.
47 W. Cai, R. D. Piner, F. J. Stadermann, S. Park, M. A. Shaibat, Y. Ishii, D. Yang, A. Velamakanni, S. J. An, M. Stoller, J. An, D. Chen and R. S. Ruoff, *Science*, 2008, **321**, 1815-1817.
48 H. C. Schniepp, J.-L. Li, M. J. McAllister, H. Sai, M. Herrera-Alonso, D. H. Adamson, R. K. Prud'homme, R. Car, D. A. Saville and I. A. Aksay, *The Journal of Physical Chemistry B*, 2006, **110**, 8535-8539.
49 L. J. Cote, F. Kim and J. Huang, *Journal of the American Chemical Society*, 2008, **131**, 1043-1049.
50 D. Pandey, R. Reifenberger and R. Piner, *Surface Science*, 2008, **602**, 1607-1613.
51 J. P. Perdew, K. Burke and Y. Wang, *Physical Review B*, 1996, **54**, 16533-16539.
52 J. P. Perdew, K. Burke and Y. Wang, *Physical Review B*, 1998, **57**, 14999-14999.
53 S. Grimme, J. Antony, S. Ehrlich and H. Krieg, *The Journal of Chemical Physics*, 2010, **132**, 154104.
54 S. Grimme, *Wiley Interdisciplinary Reviews: Computational Molecular Science*, 2011, **1**, 211-228.
55 E. R. Johnson and A. D. Becke, *The Journal of Chemical Physics*, 2005, **123**, 024101.
56 S. Grimme, S. Ehrlich and L. Goerigk, *Journal of Computational Chemistry*, 2011, **32**, 1456-1465.
57 O. A. Vydrov and T. Van Voorhis, *The Journal of Chemical Physics*, 2010, **133**, 244103.
58 W. Hujo and S. Grimme, *Journal of Chemical Theory and Computation*, 2011, **7**, 3866-3871.
59 S. F. Boys and F. Bernardi, *Molecular Physics*, 1970, **19**, 553-566.
60 A. V. Marenich, C. J. Cramer and D. G. Truhlar, *The Journal of Physical Chemistry B*, 2009, **113**, 6378-6396.
61 A. Klamt, *Wiley Interdisciplinary Reviews: Computational Molecular Science*, 2011, **1**, 699-709.
62 L. Verlet, *Physical Review*, 1967, **159**, 98-103.
63 H. J. C. Berendsen, J. P. M. Postma, W. F. v. Gunsteren, A. DiNola and J. R. Haak, *The Journal of Chemical Physics*, 1984, **81**, 3684-3690.
64 J. P. Stewart, *J Mol Model*, 2007, **13**, 1173-1213.
65 D. Cortes Arriagada, L. Sanhueza and W. Kerry, *Int. J. Quantum Chem.*, 2013.
66 D. Cortés-Arriagada, L. Sanhueza and M. Santander-Nelli, *J Mol Model*, 2013, **19**, 3569-3580.
67 F. Neese, *Wiley Interdisciplinary Reviews: Computational Molecular Science*, 2012, **2**, 73-78.
68 J.P. Stewart, Stewart Computational Chemistry, Colorado Springs, CO, USA, HTTP://OpenMOPAC.net (2012).
69 A.-R. Allouche, *Journal of Computational Chemistry*, 2011, **32**, 174-182.
70 http://www.chemcraftprog.com
71 T. Lu and F. Chen, *Journal of Computational Chemistry*, 2012, **33**, 580-592.
72 E. D. Glendening, C. R. Landis and F. Weinhold, *Journal of Computational Chemistry*, 2013, **34**, 1429-1437.
73 M. Blanchard, K. Wright, J. D. Gale and C. R. A. Catlow, *The Journal of Physical Chemistry C*, 2007, **111**, 11390-11396.
74 E. R. Johnson, S. Keinan, P. Mori-Sánchez, J. Contreras-García, A. J. Cohen and W. Yang, *Journal of the American Chemical Society*, 2010, **132**, 6498-6506.
75 J. Contreras-García, E. R. Johnson, S. Keinan, R. Chaudret, J.-P. Piquemal, D. N. Beratan and W. Yang, *Journal of Chemical Theory and Computation*, 2011, **7**, 625-632.
76 R. F. Bader, *Atoms in molecules*, Wiley Online Library, 1990.
77 A. G. Garcia, S. E. Baltazar, A. H. R. Castro, J. F. P. Robles and A. Rubio, *Journal of Computational and Theoretical Nanoscience*, 2008, **5**, 2221-2229.
78 J. Dai, J. Yuan and P. Giannozzi, *Applied Physics Letters*, 2009, **95**, 232105.
79 P. A. Denis, *Chemical Physics Letters*, 2010, **492**, 251-257.
80 A. Fukushima, A. Sawairi, K. Doi, M. Senami, L. Chen, H. Cheng and A. Tachibana, *Journal of the Physical Society of Japan*, 2011, **80**.
81 D. Cortés-Arriagada, S. Gutiérrez-Oliva, B. Herrera, K. Soto and A. Toro-Labbé, *The Journal of Chemical Physics*, 2014, **141**, -.
82 A. Fukushima, A. Sawairi, K. Doi, M. Senami, L. Chen, H. Cheng and A. Tachibana, *Journal of the Physical Society of Japan*, 2011, **80**, 074705.
83 Y. Li, Z. Zhou, G. Yu, W. Chen and Z. Chen, *The Journal of Physical Chemistry C*, 2010, **114**, 6250-6254.
84 R. C. Longo, J. Carrete and L. J. Gallego, *The Journal of Chemical Physics*, 2011, **134**, -.
85 O. Leenaerts, B. Partoens and F. Peeters, *Physical Review B*, 2009, **79**, 235440.
86 T. O. Wehling, A. I. Lichtenstein and M. I. Katsnelson, *Applied Physics Letters*, 2008, **93**, -.
87 J. Ma, A. Michaelides, D. Alfè, L. Schimka, G. Kresse and E. Wang, *Physical Review B*, 2011, **84**, 033402.